JACS
JOURNAL OF THE AMERICAN CHEMICAL SOCIETY
Communication
pubs.acs.org/JACS

Lateral Fusion of Chemical Vapor Deposited $N = 5$ Armchair Graphene Nanoribbons

Zongping Chen,[†] Hai I. Wang,[‡] Nerea Bilbao,[§] Joan Teyssandier,[§] Thorsten Prechtl,[†,∥] Nicola Cavani,[⊥,#] Alexander Tries,[†,‡] Roberto Biagi,[⊥,#] Valentina De Renzi,[⊥,#] Xinliang Feng,[▽] Mathias Kläui,[‡] Steven De Feyter,[§] Mischa Bonn,[*,†] Akimitsu Narita,[*,†] and Klaus Müllen[*,†,∥]

[†]Max Planck Institute for Polymer Research, Ackermannweg 10, D-55128 Mainz, Germany
[‡]Institute of Physics, Johannes Gutenberg-University Mainz, Staudingerweg 7, D-55128 Mainz, Germany
[§]Division of Molecular Imaging and Photonics, Department of Chemistry, KU Leuven, Celestijnenlaan, 200 F, B-3001 Leuven, Belgium
[∥]Institute of Physical Chemistry, Johannes Gutenberg-University Mainz, Duesbergweg 10-14, D-55128 Mainz, Germany
[⊥]Dipartimento di Scienze Fisiche, Informatiche e Matematiche, Università di Modena e Reggio Emilia, I-41125 Modena, Italy
[#]CNR-NANO, Istituto Nanoscienze, Centro S3, I-41125 Modena, Italy
[▽]Center for Advancing Electronics Dresden and Department of Chemistry and Food Chemistry, Technische Universität Dresden, Mommsenstrasse 4, D-01062 Dresden, Germany

Supporting Information

ABSTRACT: Bottom-up synthesis of low-bandgap graphene nanoribbons with various widths is of great importance for their applications in electronic and optoelectronic devices. Here we demonstrate a synthesis of $N = 5$ armchair graphene nanoribbons (5-AGNRs) and their lateral fusion into wider AGNRs, by a chemical vapor deposition method. The efficient formation of 10- and 15-AGNRs is revealed by a combination of different spectroscopic methods, including Raman and UV−vis-near-infrared spectroscopy as well as by scanning tunneling microscopy. The degree of fusion and thus the optical and electronic properties of the resulting GNRs can be controlled by the annealing temperature, providing GNR films with optical absorptions up to ∼2250 nm.

Graphene nanoribbons (GNRs), a new class of quasi-one-dimensional nanomaterials, exhibit unique electronic properties, distinct from graphene sheets, such as semiconducting behavior with nonzero bandgap[1−3] and strong excitonic absorption from UV into infrared range.[4,5] As the electronic band structure of GNRs relies critically on their width and edge configuration,[1,2] it is crucial to synthesize GNRs with controlled structures. In particular, GNRs with armchair edges are chemically stable and promising for application as semiconductors.[6,7] Depending on the width, armchair GNRs (N-AGNRs) can be divided into three subfamilies with atomic number $N = 3n$, $3n + 1$, and $3n + 2$ (with N the number of carbon atoms across the width of a GNR, and n an integer).[2,3] The bandgap in each subfamily scales inversely with the ribbon width, whereas the bandgaps of AGNRs in different subfamilies, but with the same n, follow a trend as $3n + 2 \ll 3n < 3n + 1$.

Up to now, AGNRs with atomic number $N = 5, 7, 9, 13$ have been synthesized by bottom-up protocols through polymerization and graphitization of different halogenated monomers on metal surfaces.[4,7−13] However, synthesis of other AGNRs has remained elusive due to the difficulty in the design and synthesis of appropriate monomers that can be efficiently polymerized and precisely cyclized on the surface. An alternative approach is lateral fusion of poly(*para*-phenylene) (PPP) chains[14] or narrower AGNRs,[15−17] which are in situ prepared on the surface from corresponding monomers. Formation of AGNRs with $N = 6$, 14, 18, and 21 has thus been observed by thermal annealing of PPP and 7- and 9-AGNRs at higher temperatures.[14−17] Nevertheless, they were mostly rather randomly and/or occasionally generated, coinciding with branching of GNRs, and studied only locally by scanning probe microscopy (SPM) techniques. This shortcoming precluded other characterization at the macroscopic level, such as by Raman and UV−vis-near-infrared (NIR) absorption spectroscopy.

Although most of the previous on-surface syntheses of GNRs have been carried out under ultrahigh vacuum (UHV) conditions, chemical vapor deposition (CVD) has recently been proven to enable a high-throughput synthesis of structurally defined GNRs.[4,8,10,18] Here we report a bottom-up synthesis and lateral fusion of 5-AGNRs by a CVD process. Efficient formation of wider AGNRs with $N = 10$ and 15 is demonstrated by Raman spectroscopy, in addition to SPM. Moreover, high-resolution electron energy loss spectroscopy (HREELS), UV−vis-NIR absorption, and ultrafast photoconductivity measurements corroborated efficient fusion of 5-AGNRs and simultaneously displayed extension of the absorption up to ∼2250 nm after annealing at higher temperatures.

We first attempted lateral fusion of 7-AGNR into 14- and 21-AGNRs under CVD conditions (see Figure S1). Although this fusion process has been reported by SPM studies under UHV

Received: May 16, 2017
Published: June 26, 2017

DOI: 10.1021/jacs.7b05055
J. Am. Chem. Soc. 2017, 139, 9483−9486

conditions,[17] we could not observe wider AGNRs by Raman spectroscopy even after annealing at 650 °C (Figure S1). We next considered fusion of 5-AGNRs, expected to be more mobile on the surface than 7-AGNR owing to the smaller width. First, efficient CVD synthesis of 5-AGNRs was established, using an isomeric mixture of 3,9-dibromoperylene and 3,10-dibromoperylene (**DBP**) as the precursor, which was prepared following our previous report (Figure 1).[10,13,19] In a

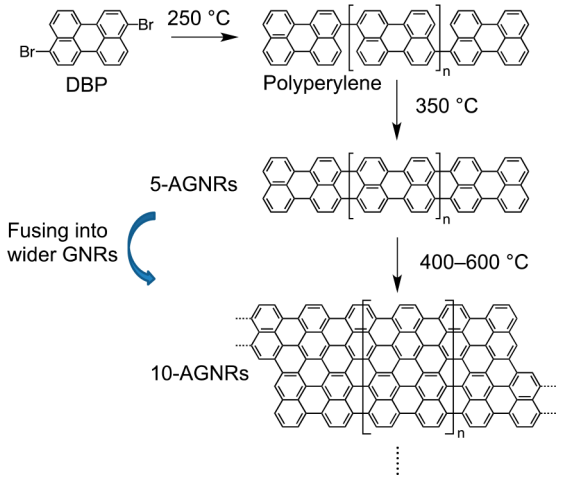

Figure 1. CVD growth of $N = 5$ armchair GNRs (5-AGNRs) and their lateral fusion to wider GNRs.

typical optimized procedure, **DBP** was sublimed at 235 °C, and deposited on an Au/mica substrate kept at 250 °C to induce homolytic carbon-bromo cleavage and polymerization of the diradical to form linear polyperylenes. Subsequent annealing at 350 °C resulted in the formation of 5-AGNRs through the surface-assisted intramolecular cyclodehydrogenation.

Although SPM can only provide very local information, which might not be representative of the majority of the sample, Raman spectroscopy is a very robust method to macroscopically characterize GNRs.[4,7−9,20,21] The resulting 5-AGNRs were first characterized by Raman spectroscopy with laser excitation at 785 nm (Figures 2, S2, and S3). The spectra reveal four main peaks at 1564, 1340, 1220, and 532 cm^{-1}, which can be assigned to G, D, edge C−H, and radial breathing-like mode (RBLM) peaks, respectively.[7,20] The RBLM of GNRs is width-specific and varies strongly with GNR width.[21] The sharp and intense RBLM peak at ~532

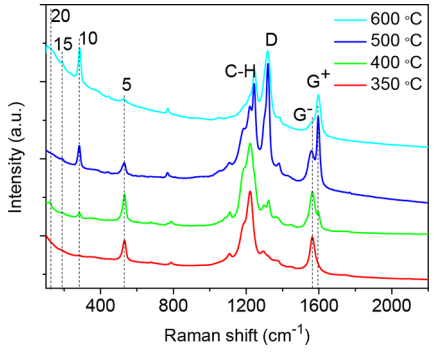

Figure 2. Raman spectra of AGNRs annealed at different temperature. The numbers 5, 10, etc. indicate the position of the RBLM peaks of respective AGNRs (excitation wavelength: 785 nm).

cm^{-1} can unambiguously be assigned to 5-AGNRs based on the value simulated by density functional theory (DFT).[21] Lateral fusion of as-formed 5-AGNRs was accomplished by annealing at higher temperatures. Notably, when the 5-AGNRs were annealed at 400 °C, wider GNRs started to form, as evidenced by the appearance of new RBLM peaks at 285, 188, and 122 cm^{-1} (Figures 2 and S2). These values were in excellent agreement with the DFT-calculated RBLM peaks for 10-, 15-, and 20-AGNRs.[9,21] Peaks from wider AGNRs than these fell outside the measurement window of our instrument. At 400 °C, the 5-AGNRs appeared to be still dominant as suggested by the ratio of the RBLM intensity, i.e., $I_{10A}/I_{5A} \approx 0.1$ (Figures 2 and S3), and scanning tunneling microscopy (STM) images (see Figure 3a,b). Annealed at 500 °C, the fusion of 5-AGNRs

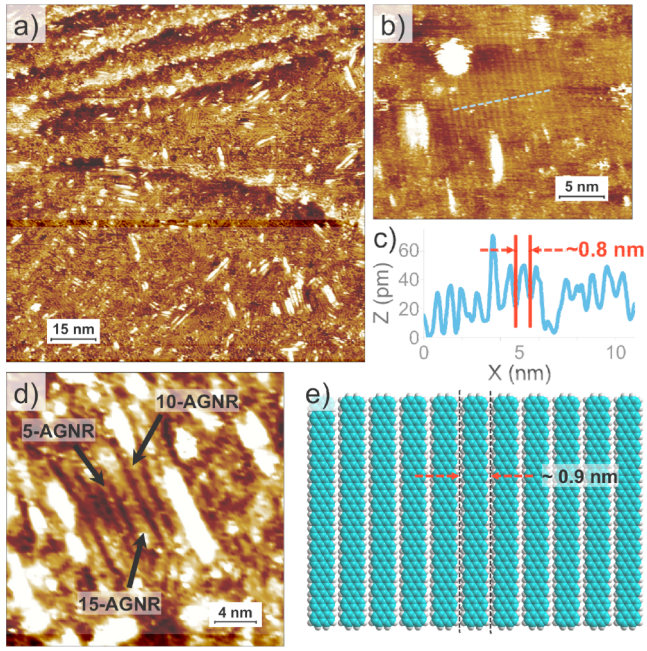

Figure 3. (a, b) STM images of the sample prepared at 400 °C showing 5-AGNR domains covering the surface of Au (111)/mica (I_{set} = 100 pA, V_{bias} = −0.2 V and I_{set} = 200 pA, V_{bias} = −0.65 V respectively). (c) Line profile along the dotted line in panel b showing a periodicity of 0.8 nm for the lamellae. (d) STM image showing the formation of broader GNRs at 600 °C (I_{set} = 200 pA, V_{bias} = −0.4 V). (e) Molecular model depicting the lamellar assembly of 5-AGNRs.

further proceeded and the RBLM peak of 10-AGNRs started to dominate ($I_{10A}/I_{5A} \approx 1.9$). Moreover, after annealing at even higher temperature of 600 °C, the RBLM of 5-AGNRs almost completely disappeared ($I_{10A}/I_{5A} \geq 10.6$), demonstrating the high efficiency of the lateral fusion of 5-AGNRs. It must be noted here that the ratio of RBLM intensities does not quantitatively reflect the ratio of the AGNRs, since the RBLM is starkly dependent on the optical absorption of the GNRs and the excitation wavelength of the measurement.[4,9] For instance, Raman excitation at 488 nm of the 600 °C sample, known to contain both 10- and 15-AGNRs, displayed significant RBLM Raman intensity only from 15-AGNRs (Figure S4).

Furthermore, the G peak shows an interesting behavior, accompanying the lateral fusion. The G peak of 5-AGNRs prepared at 350 °C splits into two peaks, namely a main G^- peak at 1563 cm^{-1} and a weak G^+ peak as a shoulder at 1596 cm^{-1}, which originates from the frequency splitting of the longitudinal and transverse optical modes in AGNRs

DOI: 10.1021/jacs.7b05055
J. Am. Chem. Soc. 2017, 139, 9483−9486

(corresponding to the E_{2g} mode in graphene).[22] For increasing annealing temperatures, the intensity of the G^+ peak increased whereas that of the G^- peak decreased. The G^+ peak was more intense after annealing at 500 °C and then became dominant at 600 °C whereas G^- was attenuated to a tiny shoulder peak, which further corroborated the high efficiency of the lateral fusion of 5-AGNRs.

Besides Raman spectroscopy, HREELS provides further evidence for the temperature-dependent GNR fusion (see Figure S5). The intensity of a so-called DUO C−H out of plane (*opla*) bending peak,[23] characteristic of the armchair edges of 5-AGNRs decreased with increasing annealing temperature, in line with the disappearance of the armchair edges at one side of the GNRs upon the lateral fusion. The emergence of a new SOLO *opla* bending peak also supports the formation of wider GNRs, because the SOLO C−H is present only in fused GNRs (see Figure S5). Additionally, the very weak C−O−C peak in HREELS and very small O 1s signal in X-ray photoelectron spectroscopy (XPS) prove the suppressed oxidation and high-quality of thus-prepared GNR samples (Figure S6).[8]

The GNR samples were next characterized by STM, revealing small organized domains of lamellar features for samples annealed at 350 and 400 °C (Figures 3 and S7). The periodicity of the lamellar features is in the range 0.7−0.8 nm, which is very close to the expected width of 5-AGNRs (0.9 nm), verifying their formation under these growth conditions. The fusion of 5-AGNRs into broader GNRs could be confirmed on samples that had been annealed at higher temperatures. For example, Figure 3d displays lamellar features of different widths for a sample annealed at 600 °C. The widths obtained from STM images correspond to 5-AGNRs (∼0.9 nm), 10-AGNRs (∼1.3 nm), and 15-AGNRs (∼1.8 nm), based on the expected widths of 0.9, 1.5, and 2.1 nm, respectively.

Interestingly, the 5-, 10-, and 15-AGNRs belong to different subgroups ($3n + 2$, $3n + 1$, and $3n$, respectively) of AGNRs and therefore possess distinctly different band structures. To study their optical properties by UV−vis-NIR spectroscopy, we have transferred multiple layers of GNR films prepared at 350, 400, 500, and 600 °C onto fused silica substrates. Notably, the 5-AGNR sample annealed at 350 °C displays an absorption maximum at ∼900 nm in the IR region and an absorption onset at ∼1400 nm, suggesting an optical bandgap of ∼0.9 eV (Figure 4a). Furthermore, the absorption maximum of the sample annealed at 400 °C redshifts to ∼1000 nm, with an extended absorption with an onset at ∼1500 nm corresponding to a lowered optical bandgap of ∼0.8 eV. This observation suggests that the 5-AGNRs prepared at 400 °C are longer than those at 350 °C, which could be due to end-end coupling of as-formed 5-AGNRs and/or higher efficiency of the cyclodehydrogenation at 400 °C, given some open bonds were present after annealing at 350 °C. It should be noted that the observed optical bandgap of ∼0.8 eV is still larger than the theoretical optical transition at 0.48 eV based on the GW-BSE method,[24] indicating that the obtained 5-AGNRs are not yet long enough to have the properties of infinite 5-AGNRs.[13]

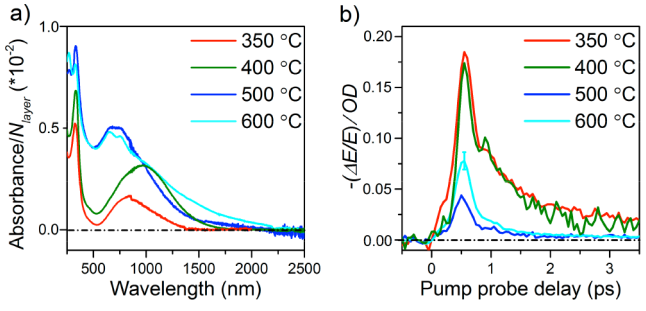

Figure 4. (a) UV−vis-NIR absorption spectra of AGNRs supported by fused silica substrates. The spectra are normalized to the number of GNR layers (N_{layer}); (b) THz photoconductivity of AGNRs. The dynamics are normalized to the optical density of the samples. The measurement error, originating from inhomogeneity of the sample, is ∼10% by measuring 5 different spots on the sample annealed at 600 °C.

In contrast, the GNR sample annealed at 500 °C exhibits a largely distinct spectrum with a substantially lower relative intensity at ∼1000 nm from 5-GNRs, and two dominant absorption peaks at ∼650 nm (∼1.91 eV) and ∼750 nm (∼1.65 eV). These two peaks can be assigned to the 10-AGNRs with a calculated optical transitions of 1.51 and 1.87 eV based on the GW-BSE method,[25] again supporting the conclusion of efficient lateral fusion at this temperature. Finally, the sample at 600 °C shows emergence of very broad absorption features extending into the infrared regime up to ∼2250 nm, which can tentatively be attributed to wider GNRs including (i) 15-AGNRs with GW-BSE-calculated optical transition of 0.73 eV;[26] and (ii) 20-AGNRs that belong to the $N = 3n + 2$ family and are expected to have an optical bandgap <0.5 eV. There is also a possibility that 5-AGNRs longer than those at 400 °C are present, considering the GW-BSE-calculated optical transition of 0.48 eV.[24] Although this sample is relatively undefined, the intense blue-shifted absorption maxima suggest that the main component is 10-AGNRs.

To obtain further insights into the lateral fusion of the AGNRs, we have investigated the photoconductivity of the samples annealed at different temperatures, using optical-pump, Terahertz-probe (OPTP) spectroscopy. Terahertz (THz) absorption (ΔE) by photogenerated free charges in the samples is proportional to the real optical conductivity $Re(\sigma)$, which can be further correlated to the intrinsic carrier mobility in GNRs by $Re(\sigma) = n*e*\mu$, where n is the carrier density and μ the mobility. To enable a qualitative comparison of carrier mobility μ among different GNR structures, we report the conductivity of the samples for the same carrier density n. This is achieved by exciting all samples by the identical incident photon-density (2.2×10^{14} cm^{-2}) and normalizing the conductivity to the optical density (OD) of each sample.

As shown in Figure 4b, the GNR samples annealed at 350 and 400 °C exhibit comparable and the highest THz conductivity among the four samples. Increasing the temperature to 500 °C led to a substantial reduction of THz conductivity, which is in line with the efficient fusion of 5-AGNRs into 10-AGNRs indicated by Raman and optical absorption spectroscopy: 10-AGNR is theoretically predicted to possess lower charge conductivity than that of 5-AGNR, due to a much larger effective mass.[2,27] Interestingly, the THz conductivity is increased again for the sample annealed at 600 °C. This result can be explained by the formation of wider, and more conductive AGNRs such as 15- and 20-AGNRs with lower bandgaps than that of 10-GNRs, as suggested by the enhanced absorption in the infrared. As such, the photoconductivity result is in a perfect agreement with the fusion process observed by Raman, STM and optical absorption characterizations.

In summary, we have achieved the bottom-up synthesis of structurally defined narrow 5-AGNRs and their efficient lateral

DOI: 10.1021/jacs.7b05055
J. Am. Chem. Soc. 2017, 139, 9483−9486

fusion into wider AGNRs through a CVD method. A combination of Raman, UV−vis-NIR absorption, and OPTP spectroscopy as well as HREELS and STM analyses evidenced (1) predominant formation of 5-AGNRs by annealing at 350−400 °C; (2) highly efficient lateral fusion into 10-AGNRs at 500 °C; and (3) formation of 15-AGNRs and probably also 20-AGNRs at 600 °C. Moreover, the remarkable optical properties of thus prepared GNR films with absorptions over visible to infrared render them highly promising for optoelectronic applications such as photovoltaics and visible-to-infrared sensing.

■ ASSOCIATED CONTENT

Supporting Information

The Supporting Information is available free of charge on the ACS Publications website at DOI: 10.1021/jacs.7b05055.

Experimental details and more characterization data: Raman, HREELS, and XPS spectra and STM images (PDF)

■ AUTHOR INFORMATION

Corresponding Authors

*bonn@mpip-mainz.mpg.de
*narita@mpip-mainz.mpg.de
*muellen@mpip-mainz.mpg.de

ORCID

Hai I. Wang: 0000-0003-0940-3984
Joan Teyssandier: 0000-0003-4369-0542
Steven De Feyter: 0000-0002-0909-9292
Mischa Bonn: 0000-0001-6851-8453
Akimitsu Narita: 0000-0002-3625-522X
Klaus Müllen: 0000-0001-6630-8786

Notes

The authors declare no competing financial interest.

■ ACKNOWLEDGMENTS

This work was financially supported by the DFG (Priority Program Graphene SPP 1459, KL1811), the Max Planck Society, the ERC Starting Grant MASPIC (No. ERC-2007-StG 208162), EC through the Graphene Flagship and the Seventh Framework Programme within the project Moquas (FP7 FET-ICT-2013-10 610449), the Office of Naval Research BRC program, KU Leuven − Internal Funds (PDM), Fund of Scientific Research-Flanders (FWO), the Belgian Federal Science Policy Office (IAP-7/05), and the State Research Centre for Innovative and Emerging Materials (CINEMA). We acknowledge Xiaoyu Jia for his support in the absorption spectroscopy measurements.

■ REFERENCES

(1) Barone, V.; Hod, O.; Scuseria, G. E. *Nano Lett.* **2006**, *6*, 2748−2754.
(2) Yang, L.; Park, C. H.; Son, Y. W.; Cohen, M. L.; Louie, S. G. *Phys. Rev. Lett.* **2007**, *99*, 186801.
(3) Son, Y. W.; Cohen, M. L.; Louie, S. G. *Phys. Rev. Lett.* **2006**, *97*, 216803.
(4) Chen, Z.; Wang, H. I.; Teyssandier, J.; Mali, K. S.; Dumslaff, T.; Ivanov, I.; Zhang, W.; Ruffieux, P.; Fasel, R.; Räder, H. J.; Turchinovich, D.; De Feyter, S.; Feng, X.; Kläui, M.; Narita, A.; Bonn, M.; Müllen, K. *J. Am. Chem. Soc.* **2017**, *139*, 3635−3638.
(5) Narita, A.; Verzhbitskiy, I. A.; Frederickx, W.; Mali, K. S.; Jensen, S. A.; Hansen, M. R.; Bonn, M.; De Feyter, S.; Casiraghi, C.; Feng, X.; Müllen, K. *ACS Nano* **2014**, *8*, 11622−11630.
(6) Wassmann, T.; Seitsonen, A. P.; Saitta, A. M.; Lazzeri, M.; Mauri, F. *Phys. Rev. Lett.* **2008**, *101*, 096402.
(7) Cai, J. M.; Ruffieux, P.; Jaafar, R.; Bieri, M.; Braun, T.; Blankenburg, S.; Muoth, M.; Seitsonen, A. P.; Saleh, M.; Feng, X. L.; Müllen, K.; Fasel, R. *Nature* **2010**, *466*, 470−473.
(8) Chen, Z.; Zhang, W.; Palma, C.-A.; Lodi Rizzini, A.; Liu, B.; Abbas, A. N.; Richter, N.; Martini, L.; Wang, X.-Y.; Cavani, N.; Lu, H.; Mishra, N.; Coletti, C.; Berger, R.; Klappenberger, F.; Kläui, M.; Candini, A.; Affronte, M.; Zhou, C.; De Renzi, V.; del Pennino, U.; Barth, J. V.; Räder, H. J.; Narita, A.; Feng, X.; Müllen, K. *J. Am. Chem. Soc.* **2016**, *138*, 15488−15496.
(9) Talirz, L.; Sode, H.; Dumslaff, T.; Wang, S.; Sanchez-Valencia, J. R.; Liu, J.; Shinde, P.; Pignedoli, C. A.; Liang, L.; Meunier, V.; Plumb, N. C.; Shi, M.; Feng, X.; Narita, A.; Müllen, K.; Fasel, R.; Ruffieux, P. *ACS Nano* **2017**, *11*, 1380−1388.
(10) Sakaguchi, H.; Kawagoe, Y.; Hirano, Y.; Iruka, T.; Yano, M.; Nakae, T. *Adv. Mater.* **2014**, *26*, 4134−4138.
(11) Nguyen, G. D.; Toma, F. M.; Cao, T.; Pedramrazi, Z.; Chen, C.; Rizzo, D. J.; Joshi, T.; Bronner, C.; Chen, Y.-C.; Favaro, M.; Louie, S. G.; Fischer, F. R.; Crommie, M. F. *J. Phys. Chem. C* **2016**, *120*, 2684−2687.
(12) Zhang, H.; Lin, H.; Sun, K.; Chen, L.; Zagranyarski, Y.; Aghdassi, N.; Duhm, S.; Li, Q.; Zhong, D.; Li, Y.; Müllen, K.; Fuchs, H.; Chi, L. *J. Am. Chem. Soc.* **2015**, *137*, 4022−4025.
(13) Kimouche, A.; Ervasti, M. M.; Drost, R.; Halonen, S.; Harju, A.; Joensuu, P. M.; Sainio, J.; Liljeroth, P. *Nat. Commun.* **2015**, *6*, 10177.
(14) Basagni, A.; Sedona, F.; Pignedoli, C. A.; Cattelan, M.; Nicolas, L.; Casarin, M.; Sambi, M. *J. Am. Chem. Soc.* **2015**, *137*, 1802−1808.
(15) Huang, H.; Wei, D.; Sun, J.; Wong, S. L.; Feng, Y. P.; Neto, A. H. C.; Wee, A. T. S. *Sci. Rep.* **2012**, *2*, 983.
(16) Kawai, S.; Saito, S.; Osumi, S.; Yamaguchi, S.; Foster, A. S.; Spijker, P.; Meyer, E. *Nat. Commun.* **2015**, *6*, 8098.
(17) Deniz, O.; Sánchez-Sánchez, C.; Dumslaff, T.; Feng, X.; Narita, A.; Müllen, K.; Kharche, N.; Meunier, V.; Fasel, R.; Ruffieux, P. *Nano Lett.* **2017**, *17*, 2197−2203.
(18) Sakaguchi, H.; Song, S.; Kojima, T.; Nakae, T. *Nat. Chem.* **2017**, *9*, 57−63.
(19) Schlichting, P.; Rohr, U.; Müllen, K. *Liebigs Ann./Recl.* **1997**, *1997*, 395−407.
(20) Saito, R.; Furukawa, M.; Dresselhaus, G.; Dresselhaus, M. S. *J. Phys.: Condens. Matter* **2010**, *22*, 334203.
(21) Zhou, J.; Dong, J. *Appl. Phys. Lett.* **2007**, *91*, 173108.
(22) Gillen, R.; Mohr, M.; Thomsen, C.; Maultzsch, J. *Phys. Rev. B: Condens. Matter Mater. Phys.* **2009**, *80*, 155418.
(23) Tommasini, M.; Lucotti, A.; Alfè, M.; Ciajolo, A.; Zerbi, G. *Spectrochim. Acta, Part A* **2016**, *152*, 134−148.
(24) Jain, M.; Chelikowsky, J. R.; Louie, S. G. *Phys. Rev. Lett.* **2011**, *107*, 216806.
(25) Prezzi, D.; Varsano, D.; Ruini, A.; Marini, A.; Molinari, E. *Phys. Rev. B: Condens. Matter Mater. Phys.* **2008**, *77*, 041404.
(26) Wang, S.; Wang, J. *J. Phys. Chem. C* **2012**, *116*, 10193−10197.
(27) Raza, H.; Kan, E. C. *Phys. Rev. B: Condens. Matter Mater. Phys.* **2008**, *77*, 245434.

DOI: 10.1021/jacs.7b05055
J. Am. Chem. Soc. 2017, 139, 9483−9486